A New Study of Bacterial Motion: Superconducting Quantum Interference Device Microscopy of Magnetotactic Bacteria

Y. R. Chemla,* H. L. Grossman,* T. S. Lee,* John Clarke,* M. Adamkiewicz,# and B. B. Buchanan#

*Department of Physics, University of California, Berkeley, and Materials Sciences Division, Lawrence Berkeley National Laboratory, and #Department of Plant and Microbial Biology, University of California, Berkeley, and Earth Sciences Division, Lawrence Berkeley National Laboratory, Berkeley, California 94720 USA

ABSTRACT The recently developed "microscope" based on a high-T_c dc SQUID (superconducting quantum interference device) is used to detect the magnetic fields produced by the motion of magnetotactic bacteria, which have permanent dipole moments. The bacteria, in growth medium at room temperature, can be brought to within 15 μm of a SQUID at liquid nitrogen temperature. Measurements are performed on both motile and nonmotile bacteria. In the nonmotile case, we obtain the power spectrum of the magnetic field noise produced by the rotational Brownian motion of the ensemble of bacteria. Furthermore, we measure the time-dependent field produced by the ensemble in response to an applied uniform magnetic field. In the motile case, we obtain the magnetic field power spectra produced by the swimming bacteria. Combined, these measurements determine the average rotational drag coefficient, magnetic moment, and the frequency and amplitude of the vibrational and rotational modes of the bacteria in a unified set of measurements. In addition, the microscope can easily resolve the motion of a single bacterium. This technique can be extended to any cell to which a magnetic tag can be attached.

INTRODUCTION

Various living microorganisms contain tiny quantities of ferromagnetic material—most commonly magnetite—that orient the host in the geomagnetic field (Spring and Schleifer, 1995; Frankel, 1984; Blakemore, 1982). One can demonstrate the presence of this material within the cell by observing its response to an applied magnetic field. In the past, because of its very weak magnetic moment, it was not possible to detect the magnetic field produced by the motion of a single living cell. However, the recently developed magnetic microscope based on a high-transition temperature dc SQUID (Black, 1995; Clarke, 1996; Lee et al., 1996) offers unprecedented sensitivity to magnetic fields produced by nearby specimens. As a result, it is now feasible to detect the various motions of a single living magnetic microorganism at room temperature and atmospheric pressure. More generally, this method should enable one to observe any cell to which a suitably coated magnetic particle can be attached.

As an example of this advance, we describe a study of the dynamics of magnetotactic bacteria (Blakemore, 1975) in an aqueous medium. First, we present a measurement of the magnetic field fluctuations produced by an ensemble of nonmotile bacteria. From this we determine the average rotational drag experienced by the cell and the average magnetic dipole moment. Next, by detecting the fluctuations from an ensemble of motile cells, we illustrate the vastly different dynamics at play. In particular, we observe vibrational and rotational modes of the bacteria associated with the flagellar motor (Lowe et al., 1987) and deduce their frequency and amplitude. Finally, we demonstrate the sensitivity of the SQUID magnetic microscope with measurements of a single moving bacterium.

Our experiments involve the species *Magnetospirillum magnetotacticum* (MS-1), which has a flagellum at each end of its spiral body (Blakemore, 1982). Each bacterium has a permanent dipole moment produced by a chain of magnetically aligned, single-domain magnetite (Fe_3O_4) particles (Frankel, 1984). This intrinsic magnet, fixed in the cell, allows the bacterium to navigate along the geomagnetic field—toward the north or south pole—to the bottom of a lake or pond. This process, known as magnetotaxis (Blakemore, 1975), together with the negative response of the bacteria to atmospheric levels of oxygen, is believed to aid these microaerobic organisms in finding the oxic-anoxic transition that provides optimum living conditions (Spormann and Wolfe, 1984). Various techniques (Kalmijn, 1981; Rosenblatt et al., 1982a,b; Esquivel and Lins de Barros, 1986; Bahaj et al., 1996; Proksch et al., 1995) have been used to measure the magnetic dipole moment and yield values ranging from 10^{-16} to 10^{-15} A · m^2.

MATERIALS AND METHODS

In our microscope, a dc SQUID fabricated from a thin film of $YBa_2Cu_3O_{7-x}$ is maintained at 77 K inside a vacuum enclosure. A room-temperature sample is positioned above the SQUID and is separated from the vaccum chamber by a 3-μm-thick silicon nitride membrane (Lee et al., 1997). The sample can be brought to within 15 μm of the SQUID. At this separation and with external magnetic fields excluded by a shield, the SQUID can resolve a dipole moment less than 10^{-17} A · m^2 in a 1-Hz bandwidth at 1 Hz. The *M. magnetotacticum* cultures are grown using a protocol provided by Bazylinski (Frankel et al., 1997). The bacteria, in ~1 ml of liquid growth medium, are placed in a microfabricated silicon cell integrated with the silicon nitride window of the microscope (Fig. 1 *A*,

Received for publication 13 October 1998 and in final form 23 March 1999.

Address reprint requests to Yann R. Chemla, 366 LeConte #7300, Department of Physics, University of California Berkeley, Berkeley, CA 94720-7300. Tel.: 510-642-3634; Fax: 510-642-1304; E-mail: ychemla@physics.berkeley.edu.

0006-3495/99/06/3323/08 $2.00

inset). Bacterial densities range from 10^7 to 10^8 ml^{-1}. Motion of the bacteria generates magnetic field fluctuations that are detected by the SQUID.

RESULTS

Nonmotile bacteria in zero magnetic field

The upper curve in Fig. 1 *A* is the power spectrum of the magnetic field noise, $S_B(f)$, generated by the Brownian rotation of nonmotile cells in a zero magnetic field. Translational Brownian motion occurs over very long time scales and does not contribute to the measured noise. To prevent settling of the bacteria, the sample is agitated every 30 min. Calculations (Debye, 1929; Lee and Chemla, unpublished calculation) show that a single nonmotile bacterium produces a Lorentzian power spectrum

$$S_B(f) \propto \frac{2\tau_o}{1 + (2\pi f\tau_o)^2} \quad (1)$$

where τ_o is the characteristic time scale of the Brownian rotation, and $1/2\pi\tau_o$ is the knee frequency. The time τ_o is $\alpha/2k_BT$ (Debye, 1929), where the rotational drag coefficient α is strongly dependent on the size of the bacterium. Modeling the bacteria crudely as rigid cylinders of length L and diameter d (neglecting the flagellum), one finds

$$\alpha = \frac{\pi\eta L^3}{3}\left[\ln\left(\frac{L}{d}\right) - \gamma\right]^{-1} \quad (2)$$

where η is the viscosity of the medium and $\gamma \approx 0.662$–$0.92d/L$ (Tirado and de la Torre, 1980). In the spectrum of Fig. 1 *A*, variation in the cell length over the population produces a distribution of Lorentzians with different τ_o. As a result, the noise falls off as $1/f^{1.9}$, not $1/f^2$. We fit the data to a distribution of Lorentzians with an average characteristic time $\bar{\tau}_o = 4.9$ s $\pm$ 0.3 s. We find the average rotational drag coefficient to be $\bar{\alpha} = (3.9 \pm 0.3) \times 10^{-20}$ N · m for $T = 290$ K. The fitting parameters are the average length $\bar{L}$ and the half-width at half-maximum (HWHM) of the distribution ΔL. Assuming $\eta = 10^{-3}$ Pa · s and $d = 0.7$ μm, we find that $\bar{L} = 3.5 \pm 0.1$ μm and $\Delta L = 0.7$ μm, values that are consistent with our optical measurements and those by other groups (Rosenblatt et al., 1982b, 1985; Esquivel and Lins de Barros, 1986; Bahaj et al., 1993, 1996). Comparable spectra were obtained from five other samples.

Nonmotile bacteria in a magnetic field

A magnetic field is applied to the sample of Fig. 1 *A* with a set of four coaxial coils. The coils are configured to produce a highly uniform field B in the sample cell. The uniform field minimizes forces $(\mathbf{m} \cdot \nabla)\mathbf{B}$ on the bacteria due to gradients ∇B. With this configuration, the uniformity $\Delta B/B$ is less than 0.1% across the entire sample. In addition, the applied field is parallel to the plane of the SQUID to within 0.1°, so that only ~0.1% of the field is sensed by the SQUID. Application of a static magnetic field $B = 100$ μT produces the second curve in Fig. 1 *A*. The noise below the knee is reduced as the nonmotile cells align with the field, and the knee frequency increases by a factor of $\epsilon = mB/k_BT$ for $mB \gg k_BT$. From the change in knee frequency we deduce $\bar{m} = (3.0 \pm 0.3) \times 10^{-16}$ A · m^2.

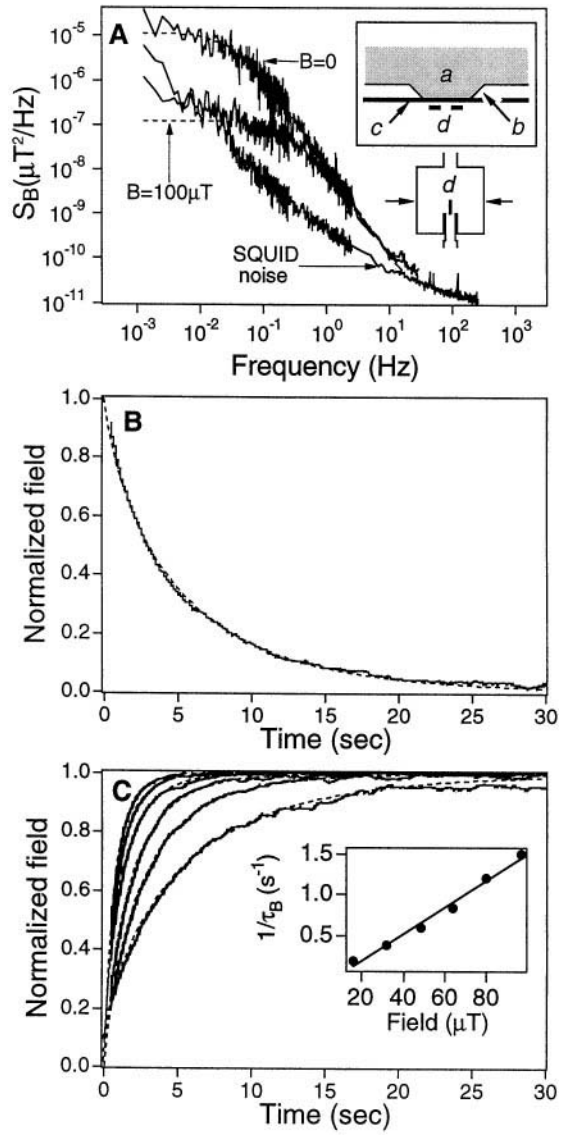

FIGURE 1 Nonmotile bacteria. (*A*) Power spectra of the magnetic field noise produced by Brownian rotation in zero magnetic field (*uppermost spectrum*) and 100 μT (*middle spectrum*). The bacteria are in growth solution (*a, inset*) contained in a silicon well (*b*) integrated with the silicon nitride vacuum window (*c*). A 500 μm × 500 μm SQUID (*d*, not to scale) is 50 μm below. The SQUID noise (*lowest spectrum*) is negligible below ~50 Hz. (*B*) Time-domain response of the bacteria to a magnetic field pulse. At $t = 0$, a uniform 96-μT field is turned off, and the magnetic field produced by the bacteria decays as their orientations randomize. The curve is fit to an exponential to obtain τ_o. (*C*) Fields of various magnitudes are turned on at $t = 0$. The bacteria orient along the field, leading to an increasing signal. Fields are 16 (*lowest curve*), 32, 48, 64, 80, and 96 μT (*uppermost curve*). Fits to exponentials (*dotted line*) yield the decay times τ_B. The inverse decay time depends linearly on the applied field (*inset*). In *B* and *C*, the signal amplitudes are normalized to unity.

An alternative method of obtaining α and m is from the time-domain response of the bacteria to a magnetic field

pulse. Fig. 1 *B* shows the decrease in the magnetic field produced by the ensemble when a 96-μT field is turned off at $t = 0$. Initially the cells are aligned with the external field, giving the sample a net dipole moment that is detected by the SQUID. When the field is removed, the orientations of the bacteria randomize, and the net dipole moment decays to zero as $\exp(-t/\tau_o)$, with $\tau_o = \alpha/2k_BT$. The curve in Fig. 1 *B* is fitted to such an exponential. Because the field pulse generates a transient (which lasts less than 100 ms) that is detected by the SQUID, data for times less than 0.5 s were ignored in the fit. We find that $\bar{\tau}_o = 4.7\text{ s} \pm 0.3\text{ s}$, and hence $\bar{\alpha} = (3.8 \pm 0.1) \times 10^{-20}\ \text{N} \cdot \text{m}$, in excellent agreement with the values from the noise measurements.

In a method similar to that of Bahaj et al. (1996), we measure m by turning on a magnetic field. Here the SQUID measures the resultant increase in the net dipole produced by the ensemble as the bacteria align with the external field. The time dependence of the signal is again exponential, with a lifetime $\tau_B = \tau_o/\epsilon = \alpha/2mB$ for $\epsilon \gg 1$. Fig. 1 *C* shows a series of decay curves obtained at different values of magnetic field; the inset shows τ_B^{-1} versus B, which yields the slope $2m/\alpha$. Using the value of $\bar{\alpha}$ determined above from the time domain measurements, we find that $\bar{m} = (3.0 \pm 0.3) \times 10^{-16}\ \text{A} \cdot \text{m}^2$, in good agreement with the value determined from the power spectrum of the noise.

Motile bacteria in zero magnetic field

Motile MS-1 exhibit very different dynamics, as illustrated in Fig. 2 *A* for zero applied magnetic field. Compared with the spectrum in Fig. 1 *A*, there are three distinct differences: the knee frequency, $1/2\pi\tau_m$, increases by an order of magnitude; the power spectrum falls off as $1/f^{\nu}$ with $\nu \approx 2.4$; and there are two peaks, at 63 and 26 Hz. The low-frequency behavior arises from the random motility of the bacteria. We have performed computer simulations (see Appendix A) of this behavior and found that τ_m is determined by both the rate at which the bacteria change direction and the average time required for them to traverse the sensing area of the SQUID. An exponent $\nu > 2$ can be reproduced by including memory effects in our simulations.

The interpretation of the peaks at 26 and 63 Hz is demonstrated in Fig. 2 *B*, where the bacteria are exposed to high levels of oxygen. There we show three spectra of the same sample at different times (curves *a* at $t = 0$, *b* at 15 min, and *c* at 75 min, offset for clarity). Atmospheric levels of oxygen contaminate the medium, causing the microaerobic cells to slow over time. As a result, the peaks in Fig. 2 *B* move to lower frequencies. Note that the two peaks move together—the ratios of frequencies and the amplitudes remain constant—indicating that they must be coupled and produced by the same source, which must be connected to the speed of the cells. In common with other motile bacteria, MS-1 propel themselves by rotating their helical flagella (Blakemore, 1982), typically at ~100 Hz (Berg, 1995); their swimming speed is proportional to the flagellar rotation rate (Lowe et al., 1987).

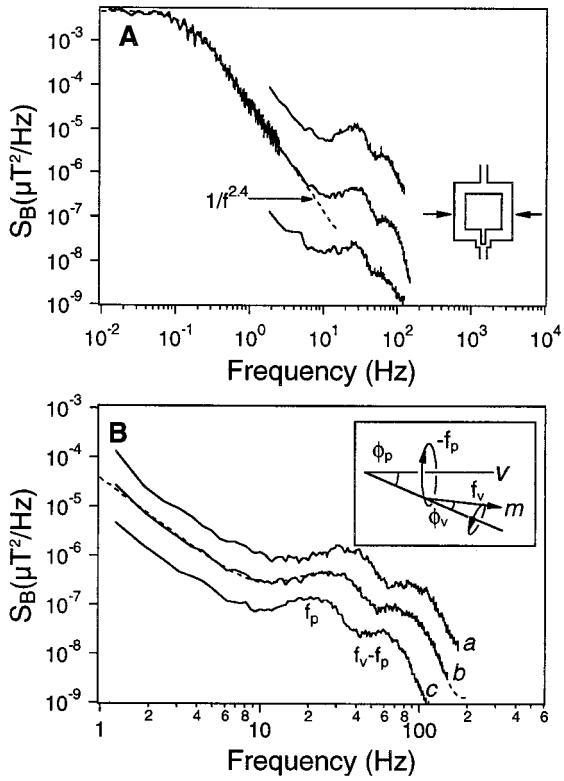

FIGURE 2 Motile bacteria. (*A*) Power spectrum of the noise produced by the random motility of the bacteria in zero magnetic field (0.01–10 Hz), and vibration (~25 Hz) and body roll (~65 Hz) of the cells due to flagellar rotation. The high-frequency peaks are reproduced in two other cultures of MS-1 (*upper and lower curves*, offset for clarity). The SQUID used in these measurements has dimensions 50 μm × 50 μm (see *inset*) and is 25 μm below the vacuum window. (*B*) High-frequency peaks. The presence of high levels of oxygen causes the ensemble to slow over time. The peaks shift to lower frequencies (curve *a* at $t = 0$, *b* at 15 min, and *c* at 75 min, offset for clarity). However, the amplitudes and ratios of frequencies remain constant. The central curve is fitted (*dotted line*). The vibration and body roll of a cell are modeled as rotations of the magnetic dipole moment m about two axes with angular amplitudes ϕ_v and ϕ_p and frequencies f_v and $-f_p$ (*inset*). Peaks in the spectrum appear at f_p and $f_v - f_p$. Gaussian distributions of frequencies account for the widths of the peaks.

Lowe et al. (1987) have observed similar peaks for *Streptococcus* optically by measuring the noise from a photocathode onto which images of the cells are projected. They attribute the two peaks to vibrations and rotations of the cell caused by its flagellum. If the length of a flagellum is not an integer number of wavelengths, an imbalance force perpendicular to the rotation axis causes the body to vibrate at the same frequency (Berg, 1983). In addition, the rotating flagellum applies a torque to the body, which responds by counterrotating at a lower frequency. If the axes of the body and flagellum are not collinear, the cell precesses (or rolls) (Lowe et al., 1987). These two coupled modes are responsible for the peaks at 63 and 26 Hz in the spectrum in Fig. 2 *A*.

From the magnitudes of the peaks it is possible to estimate the amplitudes of these modes. As a simple model, we assume that the magnetic dipole moment rotates about vibrational and precessional axes with angular amplitudes ϕ_v

and ϕ_p and frequencies f_v and $-f_p$, respectively (Fig. 2 *B*, *inset*). Physically, f_v is the rotation rate of the flagellum in the frame of the bacterium; because of the counterrotation of the body, one measures $f_v - f_p$ in the laboratory frame. Provided the angular amplitudes are small, the model reproduces the two peaks in the spectrum, with $f_p = 26$ Hz and $f_v - f_p = 63$ Hz. The widths of the peaks, due to variations in the population, are modeled by a Gaussian distribution of frequencies of width $\Delta_{v,p}$. The peak heights determine the angular amplitudes. A detailed calculation (see Appendix B) shows that it is not necessary to know the number or position of the bacteria contributing to each peak. Rather, ϕ_v and ϕ_p are determined entirely from the ratio of the spectral density at each peak at frequency $\bar{f}$ to that at low frequencies:

$$\phi^2 \approx 2\sqrt{2\pi\nu}\sin\frac{\pi}{\nu}\tau_m\Delta\cdot\frac{S_B(\bar{f})}{S_B(0)} \qquad (3)$$

The fitting parameters for curve b are $\bar{f}_v = 89.2 \pm 9.6$ Hz, $\Delta_v = 29.5 \pm 7.9$ Hz, and $\phi_v = 5.5 \pm 0.7°$ for the vibration, $\bar{f}_p = 25.9 \pm 0.2$ Hz, $\Delta_p = 10.4 \pm 0.8$ Hz, and $\phi_p = 7.0 \pm 0.4°$ for the precession. Error bars are estimated from random errors in the least-squares fitting routine and systematic fitting errors. At the highest frequencies (>150 Hz), the signal is comparable to the SQUID noise, distorting the measured spectrum. As a result, we cut the data off at some suitable frequency; however, the choice for this cutoff can systematically affect the fit. We have taken account of this effect in the error bars. Table 1 summarizes the results from the analyses of the three curves in Fig. 2 *B*. As stated above, the ratio of the peak frequencies $\bar{f}_v/\bar{f}_p$ and the peak amplitudes ϕ_p and ϕ_v are constant to within the error bars.

Motile bacteria in a magnetic field

In the presence of a static, uniform magnetic field comparable to that of the Earth, the bacteria undergo magnetotaxis. In Fig. 3 we apply a 37-μT field parallel to the SQUID plane at $t = 0$. The noise at all frequencies decreases as a function of time. The inset plots the decay in the amplitude of the precessional peak (at ~26 Hz) against time; the signal fits well to an exponential with characteristic time ~200 s. The process is reversible; when the applied field is turned off, the magnitude of the noise regains its original value. The observed decay occurs over much too long a time scale (200 s) to be due to the alignment of the bacteria with the applied field (1–10 s, as seen above). Moreover, the noise at all frequencies is affected. Because the entire spectrum is proportional to the number N of bacteria detected by the SQUID, the signal indicates that the number of cells above the SQUID decreases with time.

TABLE 1 Peak frequencies and amplitudes for bacteria in oxygen

	Curve *a*	Curve *b*	Curve *c*
$\bar{f}_p$ (Hz)	31.1 ± 0.2	25.9 ± 0.2	20.7 ± 0.2
$\bar{f}_v$ (Hz)	114.2 ± 12.3	89.2 ± 9.6	74.2 ± 8.0
$\bar{f}_v/\bar{f}_p$	3.7 ± 0.4	3.4 ± 0.4	3.6 ± 0.4
ϕ_p (°)	6.7 ± 0.4	7.0 ± 0.4	7.0 ± 0.4
ϕ_v (°)	4.6 ± 0.6	5.5 ± 0.7	5.2 ± 0.7

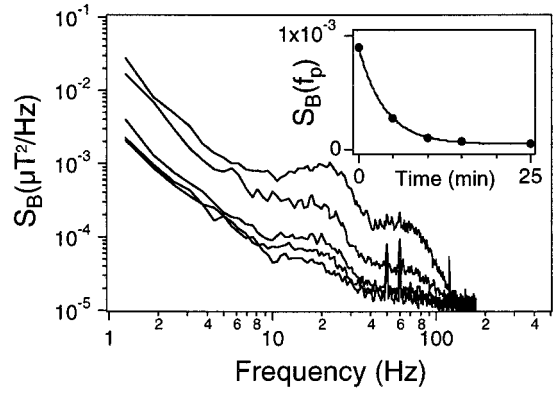

FIGURE 3 Motile bacteria in a uniform 37-μT field. The noise at all frequencies decreases as a function of time. The top spectrum is taken as the field is turned on at $t = 0$; the subsequent curves are measured at $t =$ 5, 10, 15, and, finally, 25 min. The behavior is reversed if the field is turned off. The noise above ~100 Hz is from the SQUID sensor. The magnitude of the noise at the peak frequency f_p is plotted against time in the inset. The decay fits to an exponential with time constant $\tau \approx 200$ s. The vibration and precession of the cells are not affected by the magnetic field.

Spormann and Wolfe (1984) have observed that *M. magnetospirillum*, a bipolar magnetotactic bacteria, will tend to swim toward the north or south pole of a static magnetic field. This creates regions of high cell density near the poles and low density in the center of the sample. We observe similar behavior in our experiment. The cells in Fig. 3 are swimming away from the SQUID (which is in the center of the liquid sample cell) and toward the edges. Thus the cell density over the SQUID decreases over time. The characteristic decay time can be interpreted in this context as the diffusion constant for the population. Whereas the low-frequency (i.e., long-time) behavior is clearly affected in a magnetic field, the high-frequency dynamics are not. The presence of the magnetic field does not seem to affect the vibrational and rotational modes of the bacteria, and hence the swimming speed. The ratio of the amplitudes and frequencies of the peaks in Fig. 3 is the same as in zero magnetic field.

Observations of a single bacterium

Our SQUID microscope has sufficient sensitivity to detect a single magnetotactic bacterium. Fig. 4 displays two time traces obtained from motile cells in a zero magnetic field. The upper trace is representative of most observations and consists of contributions from many bacteria. The lower trace, which we obtain only on rare occasions, is dominated by a large, oscillatory signal from a single magnetotactic bacterium. Like other bacteria, MS-1 tend to swim in orbits parallel to nearby surfaces (Frymier et al., 1995). We have

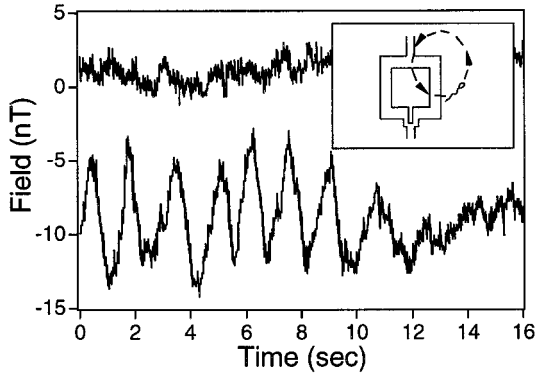

FIGURE 4 Single bacterium orbit. Typically, the field detected by the SQUID consists of small signals from many bacteria (*upper curve*, offset for clarity). Occasionally, a single bacterium swims in an orbit parallel to the silicon nitride membrane, in and out of the sensing area of the SQUID (*inset*), causing large oscillations (*lower curve*). We observe these events only when the surface of the membrane is clean and the SQUID is positioned very close to it ($\sim$15 μm).

observed such zero-field orbits under an optical microscope. We believe the oscillations in Fig. 4 are produced by a bacterium swimming parallel to the silicon nitride membrane in an orbit that passes close to the center of the SQUID (Fig. 4, *inset*). However, we cannot rule out the possibility that the signal is produced by a single cell swimming back and forth across the SQUID, although we have never directly observed this behavior. The rms noise, which we estimate by integrating the SQUID noise (Fig. 1 *A*) over the bandwidth of the traces (62.5 mHz to 25 Hz), is roughly 1.5×10^{-17} A $\cdot$ m^2. Given $m \approx 3 \times 10^{-16}$ A $\cdot$ m^2, this indicates a signal-to-noise ratio of $\sim$20, which is consistent with Fig. 4.

DISCUSSION

These experiments demonstrate the ability of the SQUID microscope to study and quantify the motility of magnetotactic bacteria. We are able to determine the average rotational drag coefficient, magnetic moment, and frequency and amplitude of the vibration and rotation of magnetotactic bacteria. These modes may play an important role in the orientation of flagellate microorganisms to stimuli (Noguiera and Lins de Barros, 1995; Crenshaw, 1993), and this determination of these amplitudes should contribute to our understanding of their relative importance in bacterial motion.

Moreover, we are able to study the effects of external disturbances on the measured parameters. The presence of high levels of oxygen causes the ensemble to slow over time, as seen by a shift of the aforementioned peaks to lower frequencies. The application of a static magnetic field causes a large-scale migration of the bacteria away from the SQUID, as evidenced by a decrease in noise at all frequencies. Whereas the low-frequency dynamics are clearly affected, the vibrational and precessional modes of the cells appear to be independent of the field.

The SQUID microscope enables us to characterize a large ensemble of bacteria (10^7 to 10^8 cells) over a wide frequency range (1 mHz to 100 Hz) in a unified set of measurements, and to provide new information on their dynamics. The ability to detect the orbit of a single bacterium with a generous signal-to-noise ratio implies that the microscope is capable of detecting the motion of a single magnetite particle with a 35-nm diameter 15 μm away in a 1-Hz bandwidth. With our more sensitive SQUIDs, one could resolve the same particle 30 μm away. While the above technique may present advantages over conventional optical methods, the measurements are made in conjunction with optical observations wherever possible to ensure a correct interpretation of the results. Although we have made extensive optical observations of the bacteria, unfortunately we are unable to visualize the cells at the same time that we measure them with the SQUID microscope. In principle, such an improvement could be made possible in the future by redesigning the current instrument.

Future studies are aimed at the dynamics and migration of magnetotactic bacteria in opaque porous media. Further studies of magnetotaxis are also planned. More generally, the SQUID microscope can be used to study any cell to which a suitably coated magnetic particle can be attached. Other potential applications include the detection of specific organelles by selective tagging.

APPENDIX A

To help interpret the power spectra for live magnetotactic bacteria, we perform computer simulations of bacterial motion in free solution and a zero magnetic field. Each simulation traces the trajectories of 2500 bacteria through 65,536 time steps of 0.01 s each. The program assumes that the bacteria move independently, because for typical densities (10^8 cells/ml) the magnetic interaction energy between bacteria is $\sim$4000 times less than the thermal energy.

The program is based on an algorithm by Frymier et al. (1993). However, whereas they simulate bacteria that run and tumble, we simulate cells that undergo continuous rotational diffusion, as observed optically for magnetotactic bacteria in zero magnetic field. For each bacterium, our program calculates the rotational diffusion coefficient $D_r = k_B T/\alpha$, where α is the rotational drag coefficient. The program chooses a random initial position and direction for the bacterium and tracks its path by sequentially rotating it through an angle $\delta\theta = (4D_r \cdot \delta t)^{1/2}$ (Debye, 1929) in a random direction and moving it a distance $\delta\mathbf{r} = \mathbf{v}\delta t$. When the bacterium reaches an edge of the well, the program repositions it at the opposite side while maintaining its original swimming direction. At each time step, the program calculates the magnetic field through the SQUID generated by the bacterium.

The program carries out this procedure separately for each bacterium, adds up the magnetic field contributions from all of the bacteria at each time step, and computes the correlation function $C_B(\Delta t) = \langle B(t + \Delta t)B(t)\rangle$, where $B(t)$ is the total field at time t. The Fourier transform of the correlation function yields the power spectrum.

For both motile and nonmotile bacteria, we find that the power spectrum has an approximately Lorentzian shape (see Fig. 5 *A*). For nonmotile bacteria, the characteristic time $\tau_o = 1/2\pi f_o$ is $1/2\bar{D}_r$. For motile bacteria, the characteristic time increases if we decrease the bacterial velocity, increase the dimensions of the SQUID, or increase the SQUID-to-sample distance. These results are consistent with an interpretation of the characteristic time as the average time it takes a bacterium to traverse the sensing area of the SQUID. To test this, we run a series of simulations in which we

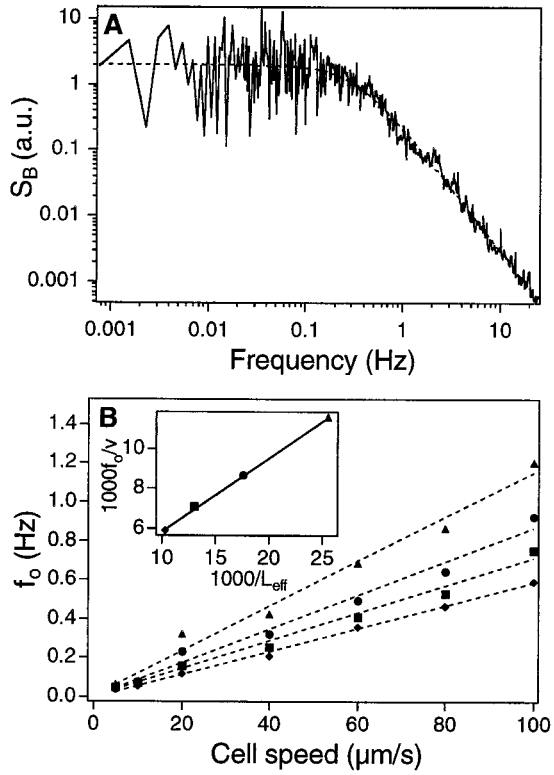

FIGURE 5 Simulations of the random motility of magnetotactic bacteria in zero magnetic field. (*A*) Example of a power spectrum generated by the simulation. The bacteria swim at an average velocity of 40 μm/s and undergo rotational diffusion; the SQUID is a 40 μm $\times$ 40 μm loop, 15 μm under the sample. No memory effects are present. The corresponding knee frequency is $f_o = 0.32$ Hz. (*B*) Dependence of the knee frequency f_o on the cell speed v and SQUID size L. For the data marked by triangles, $L = 20$ μm; circles, $L = 40$ μm; squares, $L = 60$ μm; and diamonds, $L = 80$ μm. The knee frequency depends linearly on the cell speed and inversely on the effective length L_{eff} of the SQUID (*inset*).

freeze out the Brownian rotational diffusion, causing the bacteria to swim continuously in their initial (random) direction. We treat the SQUID as a square pick-up loop of dimensions $L \times L$, and measure f_o versus v for different L. As expected, f_o scales linearly with v, and the slope decreases with increasing L (see Fig. 5 *B*).

More specifically, we postulate that $\tau \propto L_{eff}/v$, where L_{eff} is an "effective length" of the SQUID. The quantity L_{eff}, which is a function of L, takes into account the various paths that a bacterium (swimming in three dimensions) can take in passing over the SQUID. Because the sensing volume of the SQUID spreads out in a cone-like fashion above it, the further a bacterium is away from the SQUID, the longer the length it has to traverse to cross that volume. Thus the effective length is an average of the traversal lengths at each distance above the SQUID (starting at the distance between the window and the SQUID), weighted by the field contribution at that distance. If we compute L_{eff} in this way and plot f_o/v versus $1/L_{eff}$, we find a linear relation as expected (Fig. 5 *B*). For real bacteria, the characteristic time of the power spectrum is determined by both the rotational diffusion and the translational motion.

The experimental data for live bacteria exhibit a steeper slope than that of a Lorentzian. One possible explanation is nonrandom rotational diffusion, in which the bacteria retain some memory of their previous turning direction. As an example of such a process, we modify the program so that the direction of rotation at each time step is chosen from a Gaussian distribution centered on the previous turning direction with a standard deviation of $\pi/4$. The result is a power spectrum that falls off as $1/f^{2.8}$. Although this process yields a steeper slope, further study is needed to determine the specific process taking place in the experiment.

APPENDIX B

In the following we calculate the effect of the vibrational and rotational motions of the bacteria on the measured magnetic field noise power spectrum $S_B(f)$ of the SQUID. First we determine the field $B(t)$ generated at the SQUID by such motion. Then we calculate the autocorrelation function $C_B(t) \equiv \langle B(t)B(0)\rangle$ of this field and the spectral density $S_B(f)$, defined as the Fourier transform of $C_B(t)$.

Consider a bacterium at position $\mathbf{r}(t)$ measured from the center of the SQUID, undergoing the motion described in Fig. 2 *B* (*inset*). We define a bacteria (primed) reference frame such that $\hat{e}'_z$ lies along axis v in the figure, and a laboratory (unprimed) frame with $\hat{e}_z$ normal to the SQUID (see Fig. 6). The equation of motion for the magnetic dipole moment $\mathbf{m}$ in the primed frame is

$$\begin{aligned}\mathbf{m} = {} & m\hat{e}'_z[\cos\phi_p\cos\phi_v - \sin\phi_p\sin\phi_v\sin(2\pi f_v t + \delta_v)] \\ & + m\hat{e}'_x[\sin\phi_p\cos\phi_v\cos(2\pi f_p t + \delta_p) \\ & + \cos\phi_p\sin\phi_v\cos(2\pi f_p t + \delta_p)\sin(2\pi f_v t + \delta_v) \\ & - \sin\phi_v\sin(2\pi f_p t + \delta_p)\cos(2\pi f_v t + \delta_v)] \\ & + m\hat{e}'_y[\sin\phi_p\cos\phi_v\sin(2\pi f_p t + \delta_p) \\ & + \cos\phi_p\sin\phi_v\sin(2\pi f_p t + \delta_p)\sin(2\pi f_v t + \delta_v) \\ & + \sin\phi_v\cos(2\pi f_p t + \delta_p)\cos(2\pi f_v t + \delta_v)] \qquad \text{(B1)}\end{aligned}$$

where ϕ_v, ϕ_p, f_v, f_p are defined in the figure, and δ_v and δ_p are phases. The orientation of the bacteria with respect to the SQUID is arbitrary. We define θ and φ as the customary rotation angles between the laboratory and bacteria frames (see Fig. 6). The equation of motion for $\mathbf{m}$ in the laboratory frame is then easily obtained by a suitable transformation $T(\theta,\varphi)$. The result is lengthy and not particularly illuminating and will not be included here.

The field generated at the SQUID by a single bacterium is of the form $B^{(1)}(t) = \mathbf{g} \cdot \mathbf{m}$, where $\mathbf{g}$ is a geometrical factor dependent on the size of the SQUID and the position of the bacteria $\mathbf{r}(t)$. The total field detected by the SQUID due to an ensemble of N bacteria is the sum over the individual time-dependent fields:

$$B(t) = \sum_{i=1}^{N} B^{(i)}(t)$$

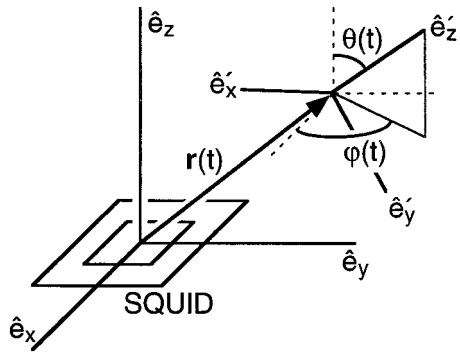

FIGURE 6 Bacterium in the laboratory (unprimed) frame. The SQUID is located at the origin of the laboratory frame, and the cell of interest is a position $\mathbf{r}(t)$ away. The bacteria (primed) frame is centered about the cell and oriented at angles $\theta(t)$, $\varphi(t)$ with respect to the SQUID. The axis $\hat{e}'_z$ is the v axis in Fig. 2 *B* (*inset*).

We will assume that there are no interactions between bacteria, so that all $B^{(i)}(t)$ are statistically independent. In that case, the autocorrelation function of the total field is the sum of the autocorrelation functions of all of the individual fields. In other words,

$$C_B(t) = \sum_{i=1}^{N} C_B^{(i)}(t) = N\langle B^{(1)}(t)B^{(1)}(0)\rangle$$

where we have replaced the sum with an average in the last step. The notation $\langle\cdots\rangle$ represents an average over all of the degrees of freedom of the system: all of the possible positions $\mathbf{r}$, orientations θ, φ, dipole moments m, frequencies $f_{v,p}$, and phases $\delta_{v,p}$ of each bacterium in the ensemble. Note that we do not average over the angles $\phi_{v,p}$, because these are presumably uniquely determined by the frequencies.

Averaged over orientation and phases, our lengthy expression simplifies greatly and reduces to two general classes of terms, one fast, the other slow. If we assume that ϕ_v and ϕ_p are small and keep only lowest-order terms, we obtain the following concise result:

$$C_B(t) = C_B(0)\{(1 - \phi_v^2 - \phi_p^2)\cdot j(t) + \langle\phi_p^2\cos(2\pi f_p t) + \phi_v^2\cos(2\pi(f_v - f_p)t)\rangle_{f_v,f_p}\cdot h(t)\} \quad \text{(B2)}$$

with $j(0) = 1 = h(0)$ and $C_B(0) = \frac{1}{3}N\langle m^2g^2\rangle_{m,r}$.

The second term is clearly responsible for the peaks at f_p and $f_v - f_p$ in the measured spectra. The functions $j(t)$ and $h(t)$ appear from the autocorrelations of the position $\mathbf{r}(t)$ and orientation $\theta(t)$ and $\varphi(t)$. They describe the swimming behavior of the bacteria—the random motility. Although the exact form of j and h is unknown at this point, the functions are responsible for the low-frequency behavior in the measured spectra. As we see in the data (Fig. 2 *A*), this behavior occurs over a characteristic time scale of $\tau_m \approx 1$ s. This is much slower than the vibration and rotation of the cell, which occur in the frequency range 10–100 Hz. Thus, in the expression above, the $j(t)$ term is "slow," whereas the $h(t)$ term is dominated by the oscillatory behavior and is "fast." When we take the Fourier transform of Eq. B2 shortly, we may set $h(t) = h(0) = 1$ with minimal error. This is equivalent to stating that the vibration and rotation occur so rapidly that we may ignore the swimming of the cell in that time scale.

The averages over f_v and f_p are carried out with a suitable probability distribution. A Gaussian peaked at frequency $\bar{f}_{v,p}$ and with width $\Delta_{v,p}$ is a reasonable assumption:

$$\langle\cdots\rangle_{f_v} \approx (2\pi\Delta_v^2)^{-1/2}\int_0^\infty df_v e^{-(f_v-\bar{f}_v)^2/2\Delta_v^2}\cdots$$

which is properly normalized in the limit that $\Delta_{v,p}/\bar{f}_{v,p}$ is adequately small.

Following the average over f_v and f_p in Eq. B2, we take the Fourier transform and obtain

$$S_B(f) = \Big\{C_B(0)(1 - \phi_v^2 - \phi_p^2)\cdot\tilde{J}(f) + \frac{\phi_v^2}{2}(2\pi\Delta_1^2)^{-1/2}\left(e^{-(f-\bar{f}_1)^2/2\Delta_1^2} + e^{-(f+\bar{f}_1)^2/2\Delta_1^2}\right) + \frac{\phi_p^2}{2}(2\pi\Delta_2^2)^{-1/2}\left(e^{(-f-\bar{f}_2)^2/2\Delta_2^2} + e^{-(f+\bar{f}_2)^2/2\Delta_2^2}\right)\Big\} \quad \text{(B3)}$$

where $\bar{f}_1 \equiv \bar{f}_p$, $\Delta_1 \equiv \Delta_p$, $\bar{f}_2 \equiv \bar{f}_v - \bar{f}_p$, and $\Delta_2^2 \equiv \Delta_v^2 + \Delta_p^2$. The function $\tilde{J}(f)$ will not be derived analytically; instead, we use an empirical function that is fitted to the data. To that end, we use a modified Lorentzian with an exponent ν:

$$\tilde{J}(f) = \frac{\nu}{2}\sin\frac{\pi}{\nu}\cdot\frac{2\tau_m}{1 + (2\pi|f|\tau_m)^\nu} \quad \text{(B4)}$$

The prefactor ensures that the sum rule $\int_{-\infty}^{\infty}S_B(f)df = C_B(0)$ is satisfied. (The sum rule is easily obtained by taking the inverse Fourier transform of S_B and setting $t = 0$.) It is trivial to verify that Eq. B2 satisfies the condition.

Equations B2 and B4 together are the fitting function for the measured spectra in Fig. 2, *A* and *B*. The angular amplitudes $\phi_{p,v}$ can be determined from the ratio of the spectral densities at the peak frequencies and at 0. Ignoring all small terms, we get

$$\phi_{p,v}^2 \approx 2\sqrt{2\pi\nu}\sin\frac{\pi}{\nu}(\tau_m\Delta_{1,2})\frac{S_B(\bar{f}_{1,2})}{S_B(0)} \quad \text{(B5)}$$

which is Eq. 3.

We thank R. B. Frankel for thoughtful comments on the manuscript, D. A. Bazylinski for the bacteria growth protocol and startup culture, H. C. Berg and D. S. Rohksar for helpful discussions, and W. Rivera for her assistance with the magnetotactic bacteria.

This work was supported by the Director, Office of Energy Research, Office of Basic Energy Sciences, Material Sciences Division of the U.S. Department of Energy under contract DE-AC03-76SF00098.

REFERENCES

Bahaj, A. S., P. A. B. James, D. C. Ellwood, and J. H. P. Watson. 1993. Characterization and growth of magnetotactic bacteria: implications of clean-up of environmental pollution. *J. Appl. Phys.* 73:5394–5396.

Bahaj, A. S., P. A. B. James, and F. D. Moeschler. 1996. An alternate method for the estimation of the magnetic moment of non-spherical magnetotactic bacteria. *IEEE Trans. Magn.* 32:5133–5135.

Berg, H. C. 1983. Random Walks in Biology. Princeton University Press, Princeton, NJ.

Berg, H. C. 1995. Torque generation by the flagellar motor. *Biophys. J.* 68:163s–167s.

Black, R. C. 1995. Magnetic microscopy using a superconducting quantum interference device. Ph.D. thesis. University of Maryland.

Blakemore, R. P. 1975. Magnetotactic bacteria. *Science.* 190:377–379.

Blakemore, R. P. 1982. Magnetotactic bacteria. *Annu. Rev. Microbiol.* 36:217–238.

Clarke, J. 1996. SQUID fundamentals. *In* NATO ASI Series, Vol. 329: SQUID Sensors: Fundamentals, Fabrication and Applications. H. Weinstock, editor. Kluwer Academic Publishers, Dordrecht, the Netherlands. 1–62.

Crenshaw, H. C. 1993. Orientation by helical motion. III. Microorganisms can orient to stimuli by changing the direction of their rotational velocity. *Bull. Math. Biol.* 55:231–255.

Debye, P. 1929. Polar Molecules. The Chemical Catalog Company, New York.

Esquivel, D. M. S., and H. G. P. Lins de Barros. 1986. Motion of magnetotactic microorganisms. *J. Exp. Biol.* 121:153–163.

Frankel, R. B. 1984. Magnetic guidance of organisms. *Annu. Rev. Biophys. Bioeng.* 13:85–103.

Frankel, R. B., D. A. Bazylinski, M. S. Johnson, and B. L. Taylor. 1997. Magneto-aerotaxis in marine coccoid bacteria. *Biophys. J.* 73:994–1000.

Frymier, P. D., R. M. Ford, H. C. Berg, and P. T. Cummings. 1995. Three-dimensional tracking of motile bacteria near a solid planar surface. *Proc. Natl. Acad. Sci. USA.* 92:6195–6199.

Frymier, P. D., R. M. Ford, and P. T. Cummings. 1993. Cellular dynamics simulations of bacterial chemotaxis. *Chem. Eng. Sci.* 48:687–699.

Kalmijn, A. J. 1981. Biophysics of geomagnetic field detection. *IEEE Trans. Magn.* 17:1113–1124.

Lee, T. S., Y. R. Chemla, E. Dantsker, and J. Clarke. 1997. High-T_c SQUID microscope for room temperature samples. *IEEE Trans. Appl. Supercond.* 7:3147–3150.

Lee, T. S., E. Dantsker, and J. Clarke. 1996. High-transition temperature superconducting quantum interference device microscope. *Rev. Sci. Instrum.* 67:4208–4215.

Lowe, G., M. Meister, and H. C. Berg. 1987. Rapid rotation of flagellar bundles in swimming bacteria. *Nature.* 325:637–640.

Noguiera, F. S., and H. G. P. Lins de Barros. 1995. Study of the motion of the magnetotactic bacteria. *Eur. Biophys. J.* 24:13–21.

Proksch, R. B., T. E. Schäffer, B. M. Moskowitz, E. D. Dahlberg, D. A. Bazylinski, and R. B. Frankel. 1995. Magnetic force microscopy of the submicron magnetic assembly in a magnetotactic bacterium. *Appl. Phys. Lett.* 66:2582–2584.

Rosenblatt, C., R. B. Frankel, and R. P. Blakemore. 1985. A birefringence relaxation determination of rotational diffusion of magnetotactic bacteria. *Biophys. J.* 47:323–325.

Rosenblatt, C., F. F. Torres de Araujo, and R. B. Frankel. 1982a. Light scattering determination of magnetic moments of magnetotactic bacteria. *J. Appl. Phys.* 53:2727–2729.

Rosenblatt, C., F. F. Torres de Araujo, and R. B. Frankel. 1982b. Birefringence determination of magnetic moments of magnetotactic bacteria. *Biophys. J.* 40:83–85.

Spormann, A. M., and R. S. Wolfe. 1984. Chemotactic, magnetotactic and tactile behaviour in a magnetic spirillum. *FEMS Microbiol. Lett.* 22: 171–177.

Spring, S., and K. H. Schleifer. 1995. Diversity of magnetotactic bacteria. *System. Appl. Microbiol.* 18:147–153.

Tirado, M. M., and J. G. de la Torre. 1980. Rotational dynamics of rigid, symmetric top macromolecules. Application to circular cylinders. *J. Chem. Phys.* 73:1986–1993.